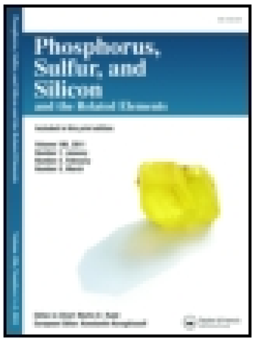

Taylor & Francis
Taylor & Francis Group

Phosphorus, Sulfur, and Silicon and the Related Elements

ISSN: (Print) (Online) Journal homepage: https://www.tandfonline.com/loi/gpss20

Synthesis, characterization and application of molecular hammock and pincer type complexes

Pratidnya Shendge , Shailza Sharma , Minati Baral , Apurva Patel , Smita Parekh & B. K Kanungo

To cite this article: Pratidnya Shendge , Shailza Sharma , Minati Baral , Apurva Patel , Smita Parekh & B. K Kanungo (2020): Synthesis, characterization and application of molecular hammock and pincer type complexes, Phosphorus, Sulfur, and Silicon and the Related Elements, DOI: 10.1080/10426507.2020.1825431

To link to this article: https://doi.org/10.1080/10426507.2020.1825431

PHOSPHORUS, SULFUR, AND SILICON AND THE RELATED ELEMENTS
https://doi.org/10.1080/10426507.2020.1825431

Synthesis, characterization and application of molecular hammock and pincer type complexes

Pratidnya Shendge[a], Shailza Sharma[a], Minati Baral[a], Apurva Patel[b], Smita Parekh[b], and B. K Kanungo[c]

[a]Department of Chemistry, National Institute of Technology Kurukshetra, Kurukshetra, Haryana, India; [b]Deparment of Biotechnology, Veer Narmad South, Gujrat University, Surat, Gujarat, India; [c]Department of Chemistry, Sant Longowal Institute of Engineering & Technology, Longowal, Punjab, India

ABSTRACT

Synthesis, characterization, coordination, bonding and electronic behavior of an ONS pincer ligand with divalent iron, cobalt, copper and zinc are described. The ligand is synthesized by condensation of dihydroxybenzaldehyde with thiosemicarbazide. The reaction of the ligand with metal ions in 1:2 (M:L) stoichiometric in identical conditions resulted in two octahedral pincer type complexes with iron and cobalt in which two ligands extend a perpendicular shape-retaining the ligand's linearity, and one trigonal bipyramidal pincer complex with zinc. For copper, the ligand preferred a bidentate coordination mode forming a square planar geometry. The structure of the copper complex can be viewed as a molecular hammock. Quantum mechanical studies at DFT level were undertaken to confirm the geometry, spectroscopic and electronic properties of all the complexes. The ability of the compounds to possess biological activity is tested against various pathogenic bacterial strains. The results show that the copper complex displays higher antimicrobial activities as compared to the ligand and other complexes. A remarkable change in the electronic spectrum of the ligand in the presence of cobalt ion in highly aqueous medium demonstrates its use as a metal sensor among a wide range of biological important metal ions.

ARTICLE HISTORY
Received 1 June 2020
Accepted 15 September 2020

KEYWORDS
Thiosemicarbazone; pincer complex; catechol; antimicrobial; electronic spectra; DFT-B3LYP

GRAPHICAL ABSTRACT

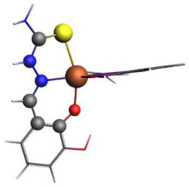

A pincer type iron complex

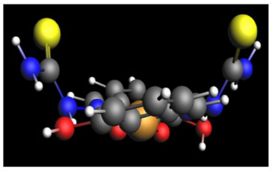

A molecular hammock type Cu(cattsc)$_2$ complex

Introduction

Thiosemicarbazones and their metal complexes have been widely studied for many years due to their promising biological activities and structural properties, and are used in the development of new therapeutic agents in medicine.[1,2] They are potential candidates that possess a broad range of biological properties including antitumor, antimalarial, antiepileptic,[3] antimicrobial,[4] and antimycotic activity.[5] Also, they have shown good antiviral activity against herpes simplex virus,[6] vaccinia and cowpox virus[7] as well as HIV.[8,9] The biological properties of thiosemicarbazones (TSC) are often related to the chelation of metal ions hence, the biological activities of TSCs can be modified or enhanced by the linkage to suitable metal ions of biological importance like Fe, Co, Ni, Cu or Zn causing no harmful effects on human healthy cells.[10] Compounds containing phenol and catechol moiety are employed in various applications such as in metal sensing, catalytic activity, and sequestering agents.[11–13] The divalent metal complexes of some Schiff bases have been studied, and are found useful in exploring important enzymatic reactions,[14] thermal and magnetic properties,[15–17] and are immensely employed in the coordination chemistry of transition metal ions.[18,19]

In designing chemosensors, the sensing of a target cation is generally achieved by the coupling of two well-defined parts: one is the cation-binding part employing various H-donor functional groups such as pyrroles, thiourea, guanidiniums, amides, catechol, and the second part is the signaling unit for the optical response.[20–23] Terdendate chelating agents that bind tightly to three adjacent coplanar sites in a meridional configuration, termed as a pincer ligand[24]

CONTACT Minati Baral minatibnitkkr@gmail.com Department of Chemistry, National Institute of Technology Kurukshetra, Kurukshetra, Haryana, 136119, India.

Supplemental data for this article is available online at https://doi.org/10.1080/10426507.2020.1825431.

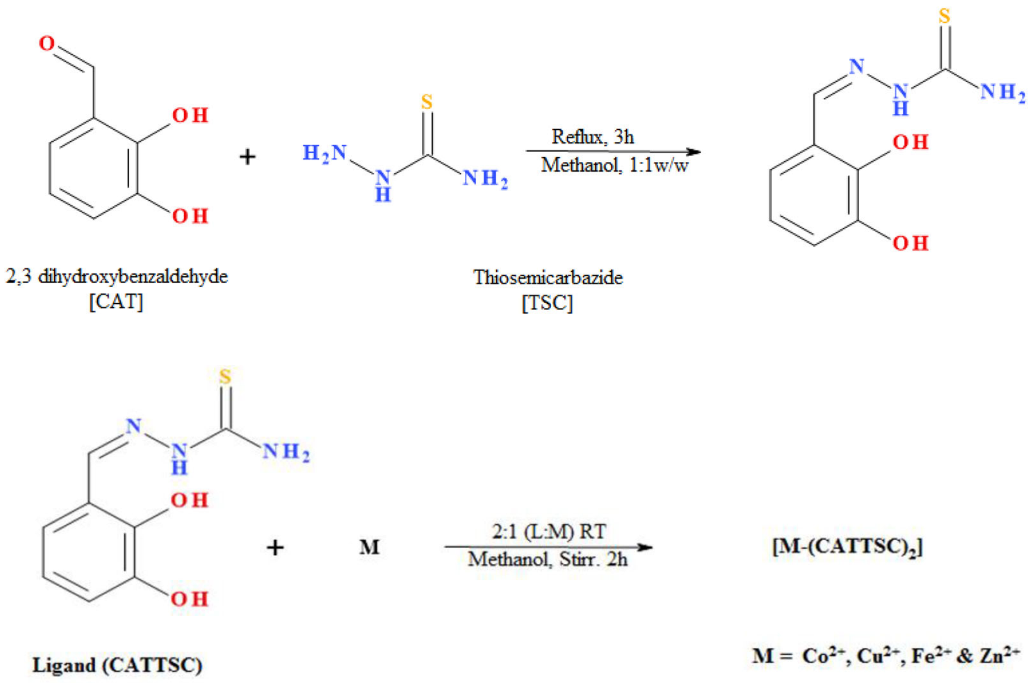

Scheme 1. Synthesis of complexes of cattsc with divalent metal ions.

which have various types of applications in organometallics and coordination chemistry,[25] particularly in catalysis. Ortho substituted arene-coupled terdentate thiosemicarbazones can be regarded as a pincer type. They form metal complexes in which the three coordinate sites and metal ion remaining in the same plane.[26] Besides, the ligand containing thiosemicarbazide as a cation binding site coupled with a catechol unit can act as a chromogenic/fluorescence selective sensor for bioactive cations. The goal of this study is to synthesize a pincer type ligand comprising a catechol and thiosemicarbazide scaffold that can also form pincer metal complexes with some bio-relevant metal ions. In this communication, the synthesis of [(Z)-(2,3-Dihydroxyphenyl)methyleneamino]thiourea, a terdentate catechol-thiosemicarbazone ligand (cattsc), and its coordination with some bioactive metal ions viz., Fe^{2+}, Co^{2+}, Cu^{2+} and Zn^{2+} are reported. The complexes are expected to have high stability and improved biological activity, enable them for applications in the field of pharmaceutics and drugs. The preparation, structural characterization, and insight on coordination behavior and electronic properties by DFT studies, and antimicrobial activities assessment of the ligand and its metal complexes are described.

Results and discussion

The ligand cattsc was synthesized by the treatment of 2,3-dihydroxybenzaldehyde with N4-substituted thiosemicarbazide in 1:1 molar ratio (Scheme 1) in methanol medium by the slightly modified literature-known procedure.[27] All the compounds synthesized are bright-colored, stable to air at room temperature and soluble in DMF and DMSO. The conductivity measurements taken in DMF at 1×10^{-3} M confirmed the uncharged nature of the ligand and metal complexes.[28] Low molecular weight compounds with no charge and very low water solubility have the advantage to be able to cross biological membranes by passive diffusion,[29] which shows the promising role of the metal chelates for suitable biological applications. The color, yield, melting point, and nature of the ligand and its metal complexes are presented in the experimental section.

IR spectra

The FT-IR spectrum of the ligand confirms condensation of 1,2 dihydroxybenzaldehyde and thiosemicarbazide by the appearance of a characteristic sharp peak for ν (-N = CH-) at 1618 cm^{-1}. Moreover, the presence of the aromatic ring can be confirmed by the appearance of the ν (-CH) band at 3086 cm^{-1}. The most characteristic vibrational frequencies and their assignments for the cattsc ligand and its metal complexes are listed in the experimental section. The assignments of the vibrational frequencies of the complexes were made by comparing them with the free ligand. The experimental IR spectra of the complexes are shown in Figures S1–S5 (Supplemental Materials). The ligand cattsc and it's all complexes remain in the thione form which is shown by the peaks around 1,377–1,340 cm^{-1} due to ν(C = S). The asymmetric stretching vibration of the thioamide group is also noticed between 855–800 cm^{-1}. In the IR spectra of the ligand and its complexes, no band was observed in the region 2,500–2,800 cm^{-1} which is due to the S–H vibration. However, a sharp band due to ν(N-NH-) is observed at 3,200–3,150 cm^{-1} in all the compounds which direct the existence of the thione group.[30,31] The presence of M-N and M-O bonds in the complexes can be confirmed by the appearance of sharp

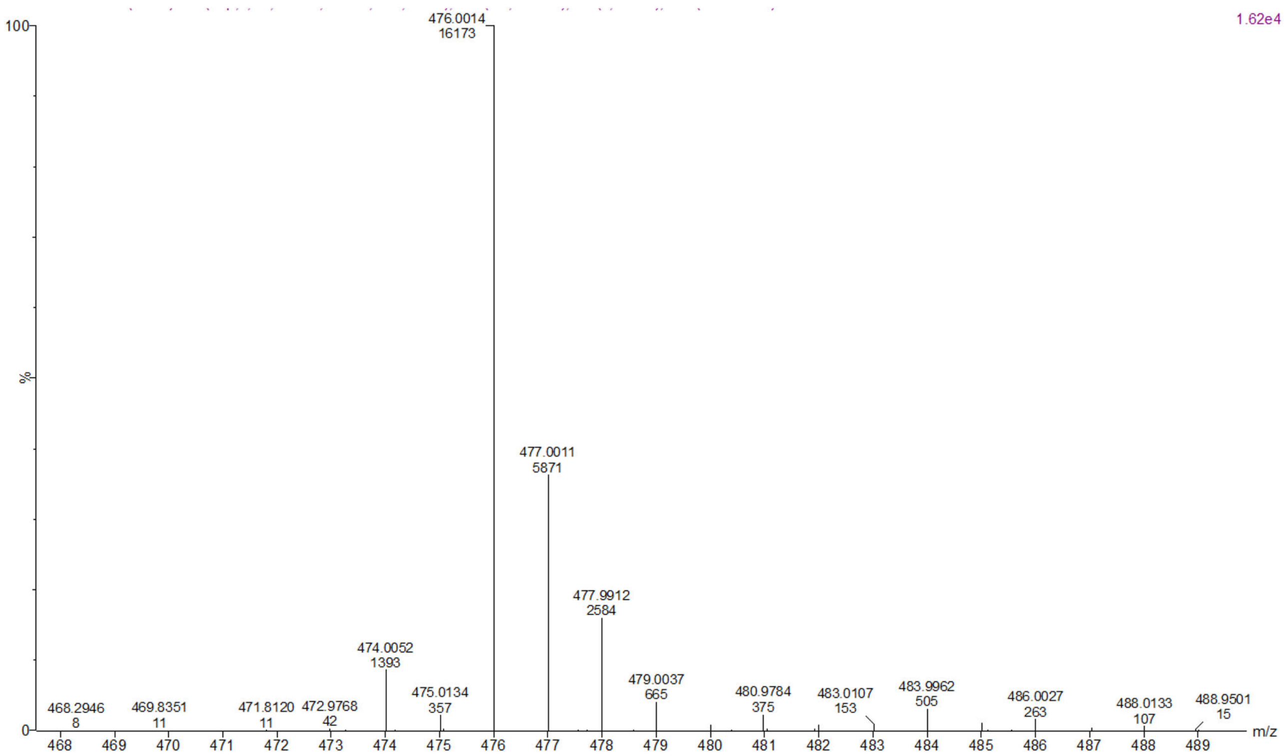

Figure 1. High Resolution ESI-MS spectrum of $Fe(cattsc)_2$. showing $[M]^+$ peak at 476.00239 u (calculated value is 476.00142 u).

and distinct peaks at 619-592 cm^{-1} and 478-418 cm^{-1},[32] which are not found in the ligand's spectrum. Deprotonated O–H due to metal coordination is difficult to identify for the presence of more than one OH group which can involve in inter and intra-molecular hydrogen bonds.[33] Broad bands in the region of 3,600 cm^{-1} are assigned to OH stretching frequency, while medium bands detected in the range of 1,093–981 cm^{-1} are allocated to the hydrazinic (N–N) bonds in the thiosemicarbazones. The azomethine $\nu(C=N)$ vibration at 1,618 cm^{-1} in the free ligand changed to 1,620–1,581 cm^{-1} after complex formation, indicating an involvement of azomethine in the metal coordination such that the electron density of the azomethine group is altered due to coordination of nitrogen to the metal atom. Moreover, this band in fact is a combination of $[\nu(C–N) + \delta(NH)]$ stretching vibrations and not a pure vibrational band of $C=N$ stretching.[31] The shifting to the higher frequency of the $\nu(N–N)$ frequency noticed in the spectra of the complexes, may be due to the electronic delocalization that occurred as a consequence of azomethine nitrogen bonding. The ligand-metal interaction through sulfur donors is confirmed by the shift in the thioamide band to lower energies along with a decrease in intensity, as compared to the respective bands of the free ligand. The vibrational frequency for M-S usually occurs at 100-300 cm^{-1}, hence could not be obtained due to spectrophotometer limitation, but a clear shift in $\nu(C=S)$ was noticed in all the four complexes except in copper, suggesting metal-sulfur coordination. Similarly, the coordination of the phenolate -O is clearly distinguished due to lowering in the $\nu(C–O)$ band as compared to the free ligand, which is further supported by the evidence of an M–O band at 480–416 $cm^{-1.}$

^1H NMR and ^{13}C NMR

The different chemical environments of protons and carbons in the ligand cattsc were determined through ^1H NMR and ^{13}C NMR spectral data recorded in deuterated dmso are given supplementary data (Figures S6 and S7). The ^1H NMR spectrum of $Zn(cttsc)_2$ complex (diamagnetic) was recorded in dmso-d_6 solvent and is given in Figure S8. The change in the position of the proton peaks in the complex is due to metal coordination. The theoretical ^1H NMR and ^{13}C NMR spectra of zinc complex are shown in Figures S9 and S10, and the spectral assignments are presented in Tables S1 and S2. The ^1H NMR spectra of other complexes could not be taken due to their paramagnetic nature and spectral broadening.[34] However, the theoretical ^1H NMR and ^{13}C NMR spectral data of the complexes were computed by the DFT method, are given in Tables S1 and S2 (Supplemental Materials).

Mass spectra

High-resolution mass spectra (HR-MS) of the ligand cttsc and all of its complexes are recorded. The respective molecular ion peaks and the calculated molecular mass of the complexes with formulation ML_2 show good agreement with each other. The mass spectrum of a representative complex, $Fe(cattsc)_2$ is shown in Figure 1 in which the peak appeared for the fragment at m/z 476.00142 u is due to the exact calculated mass 476.00239. The spectra of the ligand and other three complexes viz., $Co(cattsc)_2$, $Cu(cattsc)_2$ and $Zn(cattsc)_2$ are presented in supplementary data at Figures S11 to S14.

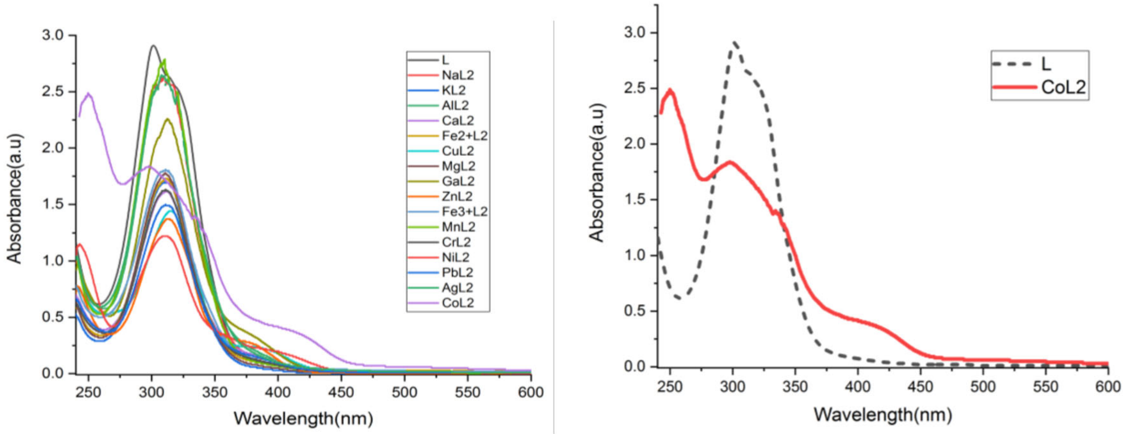

Figure 2. Electronic spectra of the ligand with different metal ions (left), and only with Co^{2+} metal ion (right).

Table 1. Electronic absorption spectral data of cattsc (L) and its metal complexes in 10^{-4} M dmso solution.

Compound	Absorption (nm)	Molar extinction coefficient (ε: $Lmol^{-1}cm^{-1}$)	Band assignment (Transitions)	Geometry (Coordination number)
L	290	2.85×10^4	$\pi \rightarrow \pi^*$	–
	310	2.70×10^4	$\pi \rightarrow \pi^*$	
FeL_2	320	1.75×10^4	IL($\pi \rightarrow \pi^*$)	Octahedral
CoL_2	250	2.52×10^4	IL($\pi \rightarrow \pi^*$)	Octahedral
	285	1.85×10^4	*d-d*+IL($\pi \rightarrow \pi^*$)	
	425	3.10×10^3	*d-d*+IL($\pi \rightarrow \pi^*$)	
CuL_2	325	1.45×10^4	IL($\pi \rightarrow \pi^*$)	Square planar
	385	2.50×10^3	*d-d*+LM CT	
ZnL_2	320	1.40×10^4	IL($\pi \rightarrow \pi^*$)	Trigonal Bipyramidal
	375	3.10×10^3	IL($\pi \rightarrow \pi^*$)	

Electronic absorption spectra

The experimental electronic spectra of cattsc and its divalent metal complexes recorded in 10^{-4} M dmso solution are presented in Figure 2; the spectral results along with the tentative spectral assignments are tabulated in Table 1. The electronic spectrum of the ligand showed a band at 290 nm with a shoulder at 310 nm, which can be attributed to intra-ligand $\pi \rightarrow \pi^*$ transitions. Only one absorption band was appeared at 320 nm due to $\pi \rightarrow \pi^*$(IL) in $Fe(cattsc)_2$ complex whereas, in the cobalt complex three bands were found in the regions 250 nm, 285 nm, and 425 nm. Involvement of d-d-transitions in addition to $\pi \rightarrow \pi^*$(IL) transitions was corroborated for the latter two bands. In $Cu(cattsc)_2$, two bands were noticed at 325 and 385 nm, ascribed to intra-ligand $\pi \rightarrow \pi^*$ and L→M charge transfer transitions but, in $Zn(cattsc)_2$ the bands obtained at 320 and 375 nm are due to $\pi \rightarrow \pi^*$(IL) transitions. Except in the case of the cobalt complex, all other species showed almost similarity in the spectral pattern. For an in-depth study on the electronic spectra, and possible transitions, theoretical calculations were performed at DFT level and discussed in the subsequent section.

Selectivity study

The selectivity in metal sensing ability of the ligand was explored where the electronic absorbance behavior of the ligand cattsc was monitored carefully with different metal ions. Further, for the purpose of other environmental/bio-applications, a highly aqueous [1:9 v/v (dmso:water)] solution was used to conduct the experiment. The electronic spectra of the ligand were investigated in the presence of a wide range of monovalent, divalent and trivalent metal ions (K^+, Na^+, Ag^+, Ca^{2+}, Co^{2+}, Cr^{3+}, Cu^{2+}, Fe^{2+}, Mg^{2+}, Mn^{2+}, Ni^{2+}, Pb^{2+}, Zn^{2+}, Al^{3+}, $Fe^{3+}$and Ga^{3+}). Amongst all the metal ions, a significant change in the ligand's absorption spectrum was detected for Co ion, which exhibited two additional bands at 250 nm and 425 nm. Similar result was obtained in pure dmso medium, but, the middle band of the ligand at 315 nm experienced a minor hypsochromic shift to 310 nm. Due to changes in polarity in the solvent medium, the bathochromic shift was observed in the ligand's absorbance from 290 to 315 nm, and also, in the presence of Co ion from 285 to 310 nm. No other metal ion could bring any noticeable change to the absorbance spectrum of the ligand and thus, approving ligand's efficient detection of Co(II) ion with high selectivity. Fluorescence sensing properties of the ligand and its selective cation recognition ability were also tested in the same solvent medium, and in the presence of the above-mentioned metal ions too, but, no distinct changes could be noticed in the fluorescence spectra.

In-silico studies

In order to obtain an insight into the molecular structures, chemical bonding, electronic and spectral properties of the ligand and four synthesized coordination compounds, molecular modeling studies were performed at DFT level using a combination of the Becke three-parameter hybrid exchange functional and Lee-Yang-Parr gradient-corrected

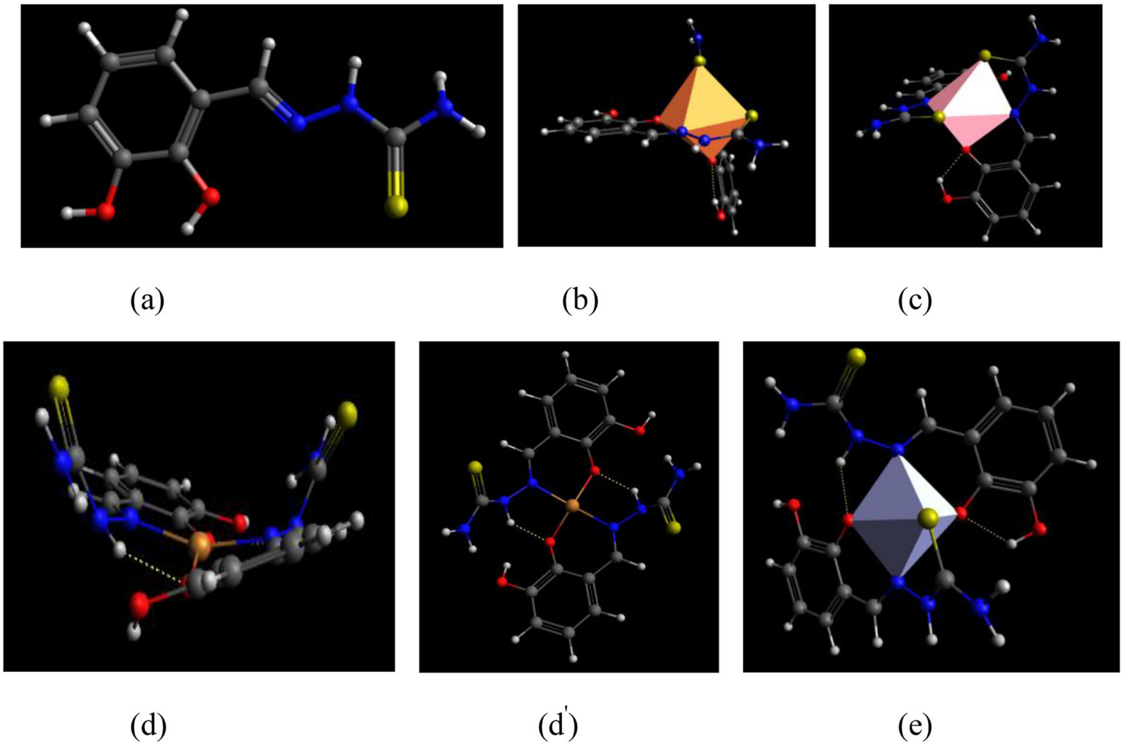

Figure 3. DFT optimized structures of (a) cattsc, (b) Fe(cattsc)$_2$, (c) Co(cattsc)$_2$, (d) and (d') Cu(cattsc)$_2$ and (e) Zn(cattsc)$_2$.

correlation functional (B3LYP). The basis set 6-311 + G(d) and 6-31 G(d)[35] were used for the ligand and metal complexes using the Gaussian 09 program[36] respectively. Although the crystal structure of the ligand was reported earlier,[37] its electronic structure and electronic spectral behavior were not described. This detailed study supplements the existing knowledge.

Molecular structures

The DFT optimized structure of cattsc extended a linear geometry (Figure 3a), which is similar to that obtained from the single-crystal X-ray diffraction study.[38] The structural parameters like bond lengths, bond angles and dihedral angles are comparable. The results are indicative that by the use of the same level of calculations, the structures of similar ligands of unknown geometry can be predicted undoubtedly.

For the metal complexes, however, the 6-31 G(d) basis set was used for the calculations. The ligand possesses two O, three N and one S donor atoms and can bind with the metal ions as bidentate (O, O; O, N or N, S, etc.), tridentate (O, O, N; O, O, S or O, N, S) or tetradentate (O, O, N, S; O, N, N, S) plausible mode of coordination. Preliminary molecular mechanics calculations using UFF forcefield of several possible tridentate modes of the ligand show that O, O, N or O, O, S type of coordination is sterically unfavorable; so also, for the tetra-coordination mode. However, the tridentate mode of coordination through ortho-O, imine N and S/amino-N is seen more promising. Study of the X-ray crystal structure of the same ligand with Ni(II) confirms a hexa-coordination environment for NiL$_2$ complex in which ortho-O, imine-N and S coordination.[38] In parallel to the same, and keeping view of the experimental results obtained in the present study, the octahedral structure was considered for all four complexes for the calculation. The x, y and z coordinates of each atom of the NiL$_2$ complex, obtained from the Cambridge Database,[39] were considered as input structure. Only the metal ions were replaced in the X-ray structure. For the input structures, spin-multiplicity of 5, 4, 2 and 1 were considered for Fe(II), Co(II), Cu(II) and Zn(II) complexes respectively corresponding to 4, 3, 1 and 0 unpaired electrons. The optimized structures were checked for the presence of any imaginary frequency to confirm that, they are the true minima. The final optimized geometries obtained for iron and cobalt complexes with coordination number six were distorted octahedral. But, the copper and zinc complexes exhibited square planar (SP) and trigonal-bipyramidal (TBP) geometry with coordination numbers four and five respectively. The optimized geometries of the complexes are given in Figure 3.

The metal-ligand (M-L) bond lengths viz., M-O, M-N and M-S, overlap population and bond orders are tabulated in Table 2. The M-L bond distances are comparable with that reported for other metal-thiosemicarbazone complexes.[38] It can be seen that the bond order ranges from 0.3- 0.5 with the overlap populations 0.07-0.2, demonstrating the bonds are coordinate covalent. The structures of iron and cobalt complexes displayed an octahedral geometry with six coordination, in which the two cattsc ligands are perpendicular to each other (Figure 4a and b), and the planar structure of the ligand practically retains its originality in the complexes with hardly any steric strain during the complex formation. The metal-ligand (donor atom) bond lengths vary and follow the trend M-O < M-N < M-S. It is apparent that, since the six M-donor atom bond lengths are unequal, the regular octahedral structure of the complexes will be

Table 2. Computed metal-ligand (coordinated atoms) bond lengths in Fe(cattsc)$_2$, Co(cattsc)$_2$, Cu(cattsc)$_2$ and Zn(cattsc)$_2$ complexes.

	M-S2		M-S3		M-O4		M-O45		M-N5		M-N10	
	Bond length (Å)	Overlap pop Bond order	Bond length (Å)	Overlap pop Bond order	Bond length (Å)	Overlap pop Bond order	Bond length (Å)	Overlap pop Bond order	Bond length (Å)	Overlap pop Bond order	Bond length (Å)	Overlap pop Bond order
Fe(cattsc)$_2$	2.752	0.075 0.234	2.628	0.091 0.306	2.042	0.136 0.380	1.952	0.157 0.475	2.165	0.123 0.308	2.165	0.119 0.306
Co(cattsc)$_2$	2.665	0.095 0.306	2.622	0.108 0.345	1.989	0.173 0.468	1.985	0.186 0.489	2.128	0.140 0.356	2.101	0.147 0.373
Cu(cattsc)$_2$	–	–	–	–	1.896	0.172 0.524	1.877	0.177 0.547	1.972	0.185 0.504	1.964	0.192 0.513
Zn(cattsc)$_2$	2.580	0.106 0.345	–	–	1.937	0.223 0.537	1.990	0.170 0.427	2.050	0.187 0.429	2.143	0.140 0.325

distorted from its O_h symmetry. It is accepted that the divalent copper can display both tetragonal distorted octahedral and square planar geometry. In the present copper complex, the two S atoms of both the cattsc ligands lie far away (~4.8 Å) from the copper center, emerging to a square planar structure, in which the central metal ion Cu, two O and two N atoms of the ligands form a square plane while rest of the atoms in the ligand undergo distortion from the planar geometry extending a Hammock shape to the molecule. A keen observation at the structure (Figure 3d) reveals the tetra-coordinated copper(II) complex as a Molecular–Hammock (swinging couch) with the two opposite hanging edges that are produced due to two C = S bonds (Figure 4d and d'). Here, it is interesting to note that, though the same initial octahedral geometry was considered as input data as in iron and cobalt complexes, the optimization process eventually resulted in a square planar structure for the copper complex. The transformation of the geometry from an octahedral to a square planar may be attributed to the effect of electronic configuration as established by the frontier molecular orbital diagram. The Cartesian coordinates of all the complexes under study are given in the supplementary data (Table S3). The structures of the complexes are in rationalization with the experimental data.

Comparison of infrared, ^{1}H NMR and ^{13}C NMR spectra. Single point calculations on the optimized structures were performed for frequency analysis and infrared spectral data under the same level of theory. Each complex molecule has 45 atoms, so 129 frequencies are expected whereas, for the ligand, 63 peaks corresponding to 23 atoms are expected. The frequencies could be identified by animating each peak. The theoretical calculated infrared spectra of the ligand and all the complexes are presented in Figure S15–S19. The significant peaks were compared with the experimental result. The regression analysis of the data for the ligand and one representative complex, Zn(cattsc)$_2$ resulted in a correlation coefficient (R^2) = ~0.99 is shown in Figure 5. The theoretical ^{1}H NMR and ^{13}C NMR spectra of the ligand (Figures S20,21) and the complexes (Table S1 and S2) were achieved by the GIAO method. The results are comparable with the experimental ones.

Frontier molecular orbital (FMO) analysis

The electronic properties and the reactivity of a molecule are mostly driven from the FMO, *i.e.*, the highest occupied molecular orbital (HOMO) and lowest unoccupied molecular orbital (LUMO). In the ligand cattsc, HOMO is the molecular orbital, MO 55 (E=-5.5 eV), mainly a nonbonding orbital comprising contribution of 75% from p_x orbital of sulfur atom S(1), 8% (s, p_x, p_y) of N(18) and 16% from -CH = N- bonding π orbital. The LUMO, MO 56 (E = -1.539 eV) is essentially an antibonding π^* orbital encompassing the six carbons of the benzene ring and two nitrogen of N-N bond, along with a very little contribution from S and N of NH_2 group. The HOMO, HOMO-1, LUMO and LUMO + 1 diagrams are shown in Figure 6, and some important data are presented in Table S4.

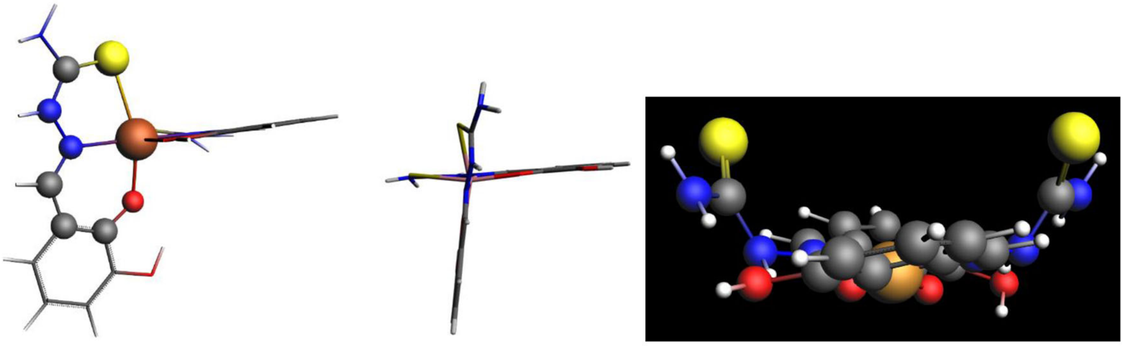

(a) Fe(cattsc)$_2$ (b) Co(cattsc)$_2$ (c) Cu(cattsc)$_2$

Figure 4. Structures of (a) Fe(cattsc)$_2$, (b) Co(cattsc)$_2$ showing two perpendicular ligands, and (c) molecular hammock structure of copper complex. The structure of iron complex viewing atoms involved in the pincer complex is also shown in Figure (a).

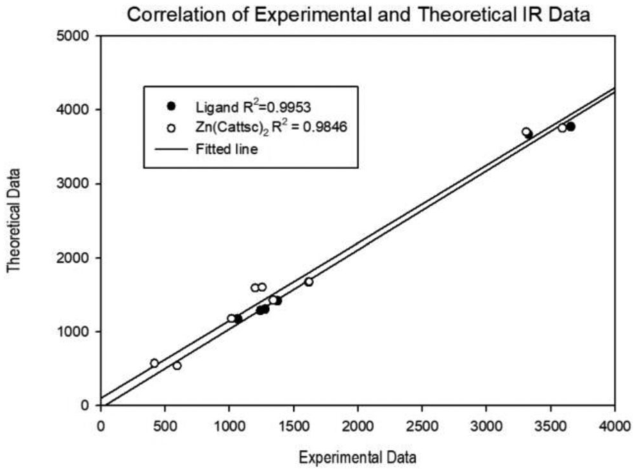

Figure 5. Correlation diagram of experimental and theoretical IR data of the ligand cattsc and Zn(cattsc)$_2$ complex.

The HOMO of Fe(cattsc) $_2$, MO 124α (E=-4.570 eV) is composed of a 4% contribution of Fe and 96% from other atoms of the ligand molecule out of which, the major contribution is from π orbital of the delocalized benzene ring and azomethine group. This MO is a singly occupied molecular orbital (SOMO). The β occupied HOMO, MO 120β (E = -4.009 eV) is composed of 61% of Fe (mainly the *d* orbital). The LUMOs are 125α (1% Fe) (E= -1.343 eV) and 121β (6% Fe) (E = -1.415 eV). They are predominantly antibonding π^*orbitals. The HOMO-LUMO gaps are 3.227 eV and 2.684 eV for α and β occupied orbitals respectively.

For the cobalt complex, the HOMO for α occupied orbitals is 124α (E = -4.575 eV) and LUMO is 125α (E = -1.338 eV). Out of two, the former is a SOMO whereas, 125α is a virtual orbital and the % of the metal contribution is 3% and 1% respectively. The HOMO consists of delocalized π-orbitals spreading over one of the benzene rings, *p* orbitals of N and *d* (dx^2-y^2, *dxy, dyz, dzx)* orbitals. The HOMO for the β-spin-orbital (MO 121β, E = -4.545 eV) is an assembly of dx^2-y^2, dz^2, *dxy*, *dyz* and *dxz* (Co: 3%) and other atoms (97%) i.e., the maximum influence of ligand π-orbitals. The LUMO β-orbital (122β) (E = -1.334 eV) contains π-orbital and cobalt *d* orbitals with a contribution of 96% and 4% respectively.

In the square planar copper complex, the HOMO 124α, E = -5.714 eV is composed of Cu (*d* orbital, 4%) and ligand (*p* and non-bonding orbital, 96%). The LUMO (125α, E = -1.835 eV) is mainly due to antibonding π^* orbital (98%) and *d* orbital (2%). β HOMO (123β, E = -5.719) has a 96% contribution from the ligand and 4% from the metal particularly for non-bonding orbital of ligand and *d* orbital of metal. The β-virtual orbital (124β) is 60% of Cu (dx^2-y^2, *dxy*) orbitals and 40% is due to antibonding MO.

With the restricted Hartree Fock calculation for the Zn complex, the HOMO (MO 124, E = -4.794 eV) is doubly occupied molecular orbital and mainly due to the π-orbitals of one of the phenyl rings having delocalized to the azomethine unit. The contribution of the metal ion is only 2%. The LUMO (MO 125, E = -1.990 eV) is mainly π^* MO (99%) and the metal contribution here is merely 1%. The energy of the two highest occupied MOs and the two lowest unoccupied MOs for the ligand and metal complexes are shown in Figure 6.

Global chemical reactivity descriptors

The structures, stability and global chemical reactivity are often described from the Kohn-Sham density functional theory using global reactivity parameters[41–50] like chemical potential(μ), global hardness (η), global softness (S), electrophilicity (ω) in addition to the well-defined ionization potential (I), electron affinity (A) and electronegativity (χ). All the parameters can be derived from the frontier molecular orbital energy and the use of Koopmans' theorem.[51] For the metal complexes, the stability order (William-Irving order) is obtained from the soft-hard acid-base (SHAB) principle. The calculated computational results obtained for the series of complexes are correlated with the said parameters (Table S5). The results indicate the stability of the complexes is Fe(cattsc) $_2$ < Co(cattsc) $_2$ < Cu(cattsc) $_2$ > Zn(cattsc) $_2$, is in agreement with the predictable order.

Time dependent density functional (TDDFT) calculations and electronic absorption spectroscopy

The electronic absorption and emission spectrum in terms of the number of bands, intensity, and electronic transition

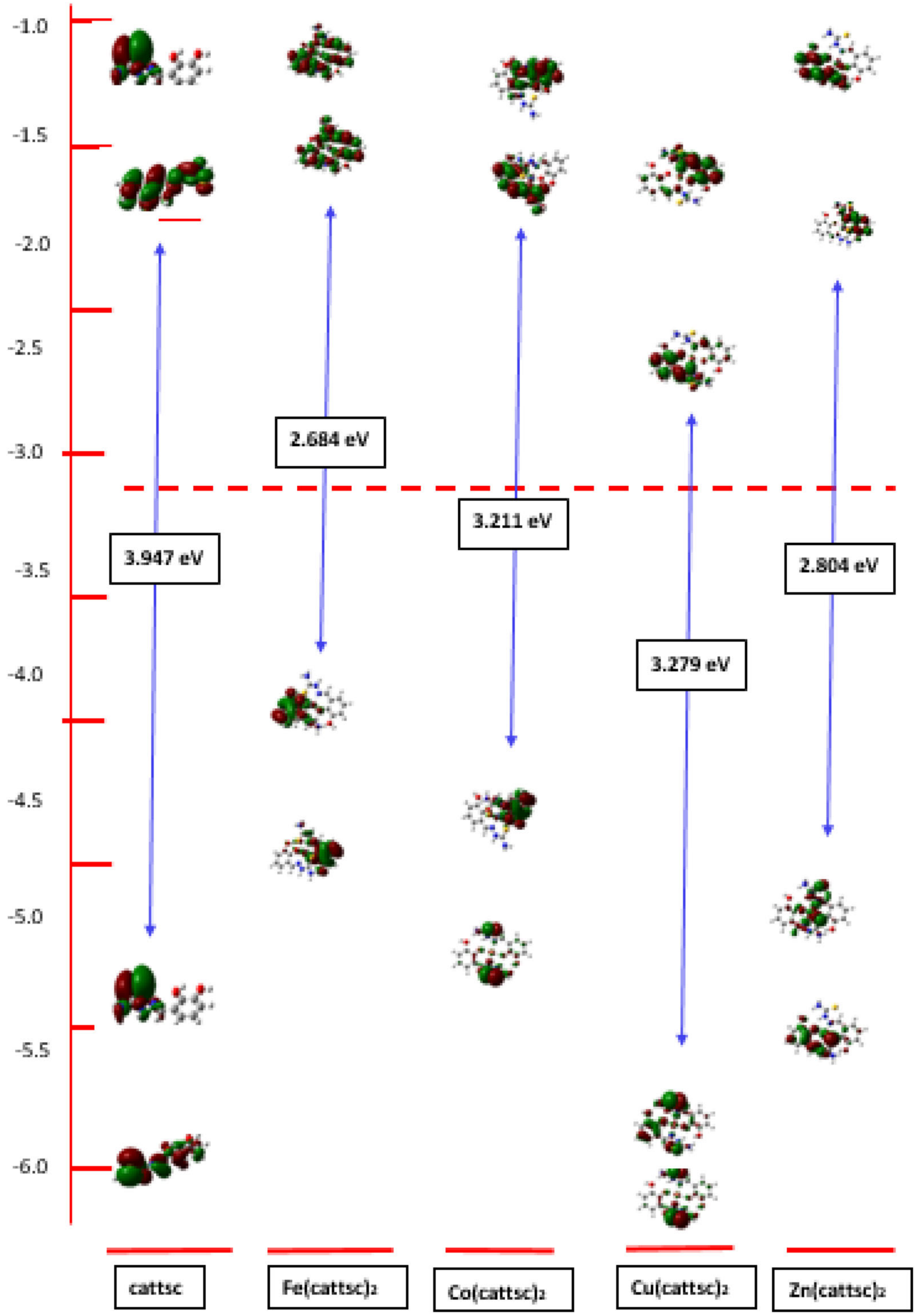

Figure 6. Molecular Energy Diagram (HOMO-1 toLUMO + 1) with density map (iso value 0.02 using Gaussview[40]) for DFT optimized structures for (a) cattsc, (b) Fe(cattsc)$_2$, (c) Co(cattsc)$_2$, (d) Cu(cattsc)$_2$ and (e) Zn(cattsc)$_2$. For iron, cobalt and copper, the orbitals containing α electrons are shown.

properties of a molecule can be obtained from TDDFT calculation.[52] In this study, the TDDFT calculations were done using the B3LYP functional and 6-31 G(d) basis set. The number of roots and states was fixed to be one and six respectively. The spectral shapes were compared with the experimental ones and the half-band-width for each case was adjusted in addition to some off-set value whenever required.

For the study of the electronic spectrum of the ligand cattsc, the half-band-width was set as 35 with no offset. The simulated electronic absorption spectrum is shown in Figure S22. Two prominent peaks could be identified from the bands of the spectrum. The absorption band at $\lambda = 270$ nm with a shoulder at $\lambda = 280$ nm is due to HOMO-3→LUMO (87.6%) and HOMO-2→LUMO (96.1%). Both the transitions can be regarded as $\pi \rightarrow \pi^*$ transitions. HOMO-2 is

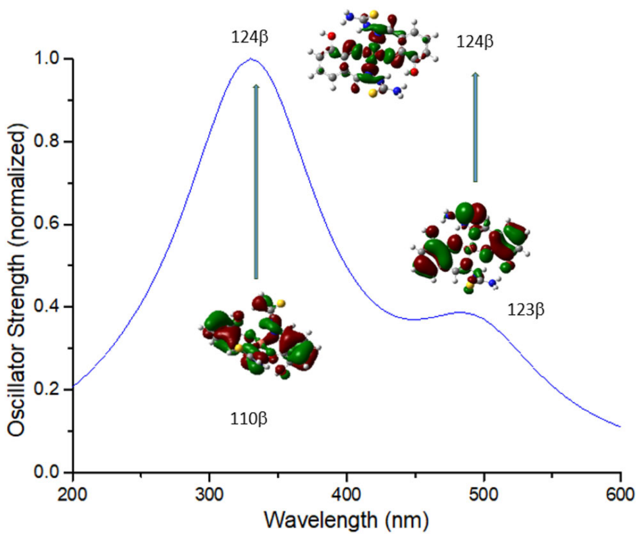

Figure 7. Theoretical electronic spectrum of Cu(cattsc)$_2$ showing the most probable transitions 110 $\beta \rightarrow$ 124 β and 123 $\beta \rightarrow$ 124 β along with their molecular orbital isosurfaces (0.02). The half-band-width = 65 and shift = -225 nm are set.

mainly comprised of π-orbitals corresponding to -C = N- and delocalized N = C=S bond.

The high-spin ($t_{2g}{}^4e_g{}^2$) iron(II) in the octahedral environment has $^5T_{2g}$ ground state, and only one transition viz., $^5T_{2g} \rightarrow {}^5E_g$ transition is expected at ~11,000 cm^{-1} (990 nm). The theoretical electronic spectrum of the iron complex displayed a band (l = 462 nm oscillator strength f = 0.011) due to HOMO → LUMO (59.7%) for α spin and HOMO-1→LUMO (19.3%) for β-spin orbitals. Studies of the orbital contribution of atomic orbitals to the molecular orbital of a particular transition imply that the transitions are mainly due to ligand orbitals, particularly the $\pi \rightarrow \pi$ * transition with the very less *d-d* transition. Another band that occurred at 630 nm (f = 0.019), is mainly due to the 120 β HOMO → 122 β (LUMO + 1) transition with 78.5% contribution. The transition of β-spin is however can be viewed primarily as M → L charge transfer (CT), since the HOMO (β-spin) is 61% Fe and 39% L, and LUMO + 1 is only 6% Fe with maximum 94% ligand orbitals. The *d-d* band can be regarded as $^5T_{2g} \rightarrow {}^5E_g$, which could be experimentally extracted by recording the spectrum in a solution of high concentration (10^{-3}M). The higher molar extension coefficient as compared to the expected value (~0.1), can be attributed to the transition to the antibonding *d*-orbital, in addition to the spin-allowed transition.

The high-energy transition of the cobalt complex is due to HOMO-1 (124 α) → LUMO + 1 (126 α) with a greater contribution (45.5%) and HOMO-1 (121 β) → LUMO (123 β) (34.1%. Since the contribution of Co is negligible (< 2%), the transition may be regarded as $\pi \rightarrow \pi^*$ transition involving the ligand orbitals particularly the phenyl ring and azomethine π orbitals. The middle range band (corresponding to the experimental band observed at 480 nm) may be regarded as HOMO-2 (119 β)→LUMO + 5 (127 β) (25.2%) and HOMO-2 (119 β) → LUMO + 3 (125 β) (21.8%). It is pertaining to mention that the contribution of (LUMO-2) β = (40% Co, 60% L), LUMO + 3 = (38% Co, 62% L) and LUMO + 5 = (47% Co, 53% L). Accordingly, the transition may be regarded as $d_{bonding} \rightarrow d_{antibonding}$ (~45%) and intraligand (IL) transition (~55%). The low-energy transition (corresponding to the experimental band at 690 nm) is due to HOMO-3 (118 β) → LUMO + 3 (125 β) (34.0%) and HOMO-3 (118 β) → LUMO + 5 (127 β) (21.2 %). Here the % contribution to MO 128 β is maximum (57%) from the cobalt ion. In this case, also, the transition may be regarded as a combination of $d_{bonding} \rightarrow d_{antibonding}$ and intra-ligand type. To rationalize the *d-d* transitions of an octahedral Co(II) complex, transitions viz., $^4T_{1g} \rightarrow {}^4T_{2g}$, $^4T_{1g} \rightarrow {}^4A_{2g}$ and $^4T_{1g} \rightarrow {}^4T_{1g}(P)$ may be highlighted, in which Co(II) has $t_{2g}{}^5e_g{}^2$ configuration with the ground state term $^4T_{1g}$. The $^4T_{1g} \rightarrow {}^4A_{2g}$ band is often hidden by $^4T_{1g} \rightarrow {}^4T_{1g}(P)$ transition and is of lower intensity since in the strong field limit is a two-electron jump. The bands are characterized by in the region $^4T_{1g} \rightarrow {}^4T_{2g}$: 6500-10,000 cm^{-1} (extinction coefficient, $\varepsilon = 5 - 40$); $^4T_{1g} \rightarrow {}^4T_{1g}(P)$: 15,000-22,000 cm^{-1} (ε = 15-60). The calculated transitions do not confirm any one of the above transitions in the complexes, as no electron was excited from any lower energy up to the SOMO *d* orbital, i.e., MO level 124α.

Copper(II) has a ground state ^2E_g in the O_h surroundings with electronic configuration $t_{2g}{}^6e_g{}^3$; however, due to the unsymmetrical electron distribution in $^{\text{e.g.,}}$ level, the symmetry is lowered resulting tetragonal distortion, known as Jahn Teller distortion. Removal of two axial ligands from the z-axis, upshots a square planar geometry (D_{4h}). According to the selection rules, the transition from the lowest energy level $d_x{}^2$-y^2 (b_{1g}) to dz^2 (a_{1g}), *dxz* and *dyz (e.g.,)* are expected in addition to the intra-ligand(IL) and charge transfer (CT) transitions. Three types of *d-d* transitions, three CT and two IL transitions have been observed in some copper(II) thiosemicarbazone complexes. Comparison of the experimental spectrum of Cu(cattsc)$_2$ with the six spectral peaks obtained theoretically, resulted in two bands by considering half-band-width of 65. The highest energy band at 325 nm is due to 110 β → 124 β (31.9%) and 111 β →124 β (19.4%) transitions. The MO 110 β (68% Cu, 32% L) and 111 β (64% Cu, 36% L) are metal and ligand orbitals. The MO 124 β is LUMO and it may be noted that the MO 124 is a single occupied molecular orbital (SOMO), i.e., 3dx^2-y^2 orbital. Hence, this band is regarded as a combination of both L→ M charge transfer (CT) and *d*→*d* transition (*e.g.,*→ b_{1g}). The lower energy band (exp: ~390 nm) is due to 123 β → 124 β transition (51.6%); specifically, a *d-d* ($dxy \rightarrow dx^2$-y^2) transition. The theoretical electronic spectrum along with the assigned transition is presented in Figure 7. The two bands in the theoretical electronic spectrum of zinc complex are due to 124 (HOMO) → 126 (LUMO + 1) (100%) and 121 (HOMO-3) → 125 (LUMO) (97.4%) and 122 (HOMO-2) → 125 LUMO) (2.6%) transitions. The MO 121 and 122 are bonding π MOs whereas, MO 125 is an antibonding π^* orbital. MO 123 is a non-bonding molecular orbital. Both the observed transitions are regarded as $\pi \rightarrow \pi^*$ transitions of intra-ligand (IL) nature. Obviously, due to a completely filled *d* orbital configuration, no *d-d* transitions are possible.

The simulated electronic spectra, probable transitions along with their assignments and the orbital diagrams of all involved MOs of cattsc and its complexes are shown in Figure S22 and Table S6.

In vitro and antimicrobial assays

The ligand and its all complexes were tested against four bacterial species: *Staphylococcus aureus*, *Escherichia coli*, *Psuedomonas aeruginosa and Bacillus subtilis* to evaluate their antibacterial activity. The species were maintained in Luria-Bertani (LB) medium at − 20 °C. Each stock-culture (0.5 mL) was added to 10 mL of LB broth; cultures were kept for 24 h at 36 °C ± 1 °C and the purity of cultures was checked after 8 h of incubation. After then, the bacterial suspension inoculum was diluted to 10^8 CFU/mL (turbidity = McFarland barium sulfate standard 0.5) by using a sterile physiological solution. Here the paper disk diffusion method was adopted for the study; the stock solution of the extract was prepared by dissolving the known quantity of the extract in dmso solvent (1 mL). 20 μL of each test was impregnated into 6 mm diameter sterile blank disks. 5 μL of the extract was marked alternately on both sides of the disks, permitted to dry before the next spotting (5 μL) for better impregnation. All disks were completely dried before the application on the bacterial lawn. Distilled water-loaded disks were employed as negative controls and tetracycline antibiotic disks as positive controls for all four strains. Antibacterial action was estimated by measuring the diameter of the inhibition region around the disks, the procedure was repeated for three times. The bacterial activity was expressed as the mean area of inhibition diameters (mm) produced by the leaf extract.[53]

From the inhibition zone, the susceptibility limit of the microorganisms against the testing molecules was predicted (Table S7). The bacterial strains indicated diverse susceptibilities to these compounds, but a significant percentage of the tested bacterial strains demonstrated high resistance except *P. aeruginosa*. The copper complex showed noticeable resistance against *Staphylococcus aureus* and *Escherichia coli* whereas, the cobalt complex was more resistant against *Bacillus subtilis*. The compounds were first subjected to a preliminary screen using the paper disk diffusion assay and based on their activity, those compounds that showed broad-spectrum activity were selected for further study.

MIC And MBC. A modification of the dilution method for estimating MIC and MBC was used. Few colonies of respective bacteria were inoculated in 20 ml LB broth, following incubation at 36 °C ± 1 °C overnight. After growth, the absorbance of bacterial culture was taken at 600 nm. The concentration of strains was fixed as 1×10^6 CFU/ml. 100 µl of this suspension was added in 11 wells of all rows of 96-well plate (1×10^4 CFU/ml). 100 µl of stock solution of given compounds were added in first well and then serial two-fold dilution upto10th well in the row. Growth control was prepared in the 11th well of each row with just bacterial suspension and LB broth (no drug added). Sterility controls are the LB broth medium alone taken in the 12th well of each row and the extract color wells comprised of the incubation mixture with no bacterial inoculum (to prevent interference of the color of the plant extract in the outcomes). The incubation of the plates was done at 37 °C (24 h). The appearance of turbidity is an indication of bacterial growth, and no turbidity formation is often interpreted as antibacterial activity. The MIC value was taken as the lowest concentration of the compounds which brought complete inhibition (100%) of bacterial growth in the current experimental situations. The MBC was determined by extracting 100 µl of broth aliquots from each well showing no turbidity (no growth), and then incubated in LB agar in similar condition as above. Bacterial viability controls included aliquots taken from growth control wells. The MBC was defined as the lowest concentration of assayed samples which produced a 99.9% reduction in CFU ml^{-1} as compared with the control.[54]

The MIC values of compounds are compared with the MIC values of established drugs viz., gentamicin, tetracycline, amoxicillin, ampicillin, erythromycin and cloxacillin against tested microorganisms,[38,55,56] and are presented in Table S8. The MIC values of all the compounds toward *Escherichia coli* are higher than that of compared standard drugs. The inhibitory level of the ligand is comparable with gentamicin, tetracycline and erythromycin only against *Bacillus subtilis.* The ligand cattsc showed prominent antibacterial activity against *Bacillus subtilis* resulting MIC value = 1.00 µg/ml which is almost similar to gentamicin (MIC 0.8 µg/ml), and higher than tetracycline (MIC 2.5 µg/ml) and erythromycin (MIC 1.25 µg/ml). $Cu(cattsc)_2$ also demonstrated higher inhibitory power against *Staphylococcus aureus* (MIC 46.88 µg/ml) and can be compared with amoxicillin (MIC >100 µg/ml), ampicillin (MIC >100 µg/ml) and cloxacillin (MIC >100 µg/ml) drugs.

Experimental

Materials and measurements

2,3-Dihydroxybenzaldehyde(Catechol), thiosemicarbazide and metal salts were obtained from Sigma-Aldrich. All the solvents used in the reaction were procured from CDH and used as received. FT-IR spectra were recorded on an IR Affinity-1S Shimadzu spectrophotometer as KBr pellets in the frequency range of 4,000–400 cm^{-1}. ^{1}HNMR and ^{13}CNMR spectra were taken in deuterated DMSO-d_6 on Bruker Avance Neo 500 MHz NMR Spectrometer from SAIF, Chandigarh. Melting points (mp) were determined with the Navyug India melting point apparatus and the thermometer was uncorrected. Conductance measurements of the compounds were carried out by Digital Cond. Meter G-3001 HPG Systems in 10^{-3}M DMF solution. The metal and sulfur were estimated by gravimetric method.[57] Electronic absorbance spectra ware taken in Thermo Scientific Evolution 201 UV-vis Spectrophotometer and Mass spectra were obtained in Waters, Q-TOF Micromass (HR-MS ESI) instrument from SAIF Chandigarh.

Theoretical calculations are made using Gaussian 09 software. The optimized molecular structures are obtained using the Functional Density Theory (DFT). The level of calculation used is B3LYP with basis set 6-311 G(d,p) and 6-31 G(d). The calculations are carried out in the gaseous phase.

Synthesis of Fe(cattsc)$_2$

cattsc (2 g, 9.48 mmol, 2.02 eq.) was dissolved in methanol (10 mL) to which a solution of $(NH_4)_2SO_4.FeSO_4.6H_2O$ (1.84 g, 4.69 mmol, 1 eq.) in methanol (5 mL) was added slowly. The reaction mixture was stirred for 2 h at room temperature. By reducing the volume of the solvent by rota-evaporator, gray color precipitates were obtained, filtered, washed multiple times with diethyl ether to ensure removal of impurities, and dried in vacuum. Molecular formula: $Fe.C_{16}H_{16}N_6O_4S_2$; Yield: 85%; Color: Gray; M.P (°C): 178; Solubility: DMF, DMSO; Conductance ($\Omega \times 10^{-3}$): 40.5; HR-ESI MS: $[M]^+$ calcd 476.00239, obsd 476.00142; Elem anal. % for Fe(cattsc)$_2$: calcd Fe 11.72, S 13.46, obsd Fe 11.68, S 13.42; IR (ν cm^{-1}): 3605 (OH), 1612 (C=N), 1201(C-N), 1340 (C=S), 3292 (N-H), 1280 (C-O), 981(N-N), 418 (Fe-O) and 592 (Fe-N).

Synthesis of Co(cattsc)$_2$

cattsc (2 g, 9.48 mmol, 2.03 eq.) was dissolved in methanol (10 mL) and to this, a solution of $CoCl_2.6H_2O$ (1.11 g, 4.67 mmol, 1 eq.) in methanol (5 mL) was added. The mixture was stirred for 2 h at room temperature. A dark brown solution was obtained, which was concentrated by a rota-evaporator under reduced pressure to give precipitates. The brown color product was filtered, washed thoroughly with diethyl ether, and dried in vacuum. Molecular formula: $Co.C_{16}H_{16}N_6O_4S_2$; Yield: 85%; Color: Brown; M.P (°C): >300; Solubility: DMF, DMSO; Conductance ($\Omega \times 10^{-3}$): 40.5; HR-ESI MS: $[M]^+$ calcd 479.00065, obsd 478.98316; Elem anal.% for Co(cattsc)$_2$: calcd Co 12.29, S 13.38, obsd Co 12.21, S 13.33; IR (ν cm^{-1}): 3510 (OH), 1608 (C=N), 1255 (C-N), 1348 (C=S), 3298 (N-H), 1307(C-O), 1093 (N-N), 478 (Co-O) and 613 (Co-N).

Synthesis of Cu(cattsc)$_2$

To a solution of cattsc (2 g, 9.48 mmol, 2.02 eq.) in methanol (10 mL), $CuSO_4.5H_2O$ (1.17 g, 4.68 mmol, 1 eq.) in methanol (5 mL) was added dropwise. The reaction mixture was stirred well for 2 h at normal room temperature, after then its volume was reduced to half by a rotary evaporator under reduced pressure to obtain black precipitates. The crude product of copper complex was filtered, washed repetitively with diethyl ether to separate impurities, and dried in vacuum. Molecular formula: $Cu.C_{16}H_{16}N_6O_4S_2$, Yield: 87%; Color: Black; M.P (°C): 197; Solubility: DMF, DMSO; Conductance ($\Omega \times 10^{-3}$): 27.0; HR-ESI MS: $[M+H]^+$ calcd 484.00432, obsd 484.00523; Elem anal.% for Cu(cattsc)$_2$: calcd Cu 13.13, S 13.25, obsd Cu 13.08, S 13.21; IR (ν cm^{-1}): 3588 (OH), 1581 (C=N), 1112 (C-N), 1377 (C=S), 3300 (N-H), 1255 (C-O), 1062 (N-N), 418 (Cu-O) and 619 (Cu-N).

Synthesis of Zn(cattsc)$_2$

The ligand catts (2 g, 9.47 mmol, 2.02 eq.) was taken in methanol (10 mL). To this, a solution of $Zn(CH_3COOH)_2.2H_2O$ (0.51 g, 4.68 mmol, 1eq.) in methanol (5 mL) was added in 1:2 stoichiometry. The mixture was stirred for 2 h at room temperature. The solution was reduced to half by rota-evaporation to give a yellow product of Zn complex which was filtered, washed multiple times with diethyl ether, and dried in *vacuo*. Molecular formula: $Zn.C_{16}H_{16}N_6O_4S_2$, Yield: 88%; Color: Yellow; M.P (°C): 181; Solubility: DMF, DMSO; Conductance ($\Omega \times 10^{-3}$): 13.5; HR-ESI MS: $[M]^+$ calcd 483.99659, obsd 484.00522; Elem anal.% for Zn(cattsc)$_2$: calcd Zn 13.46, S 13.20, obsd Zn 13.43, S 13.17; IR (ν cm^{-1}): 3590 (OH), 1620 (C=N), 1201(C-N), 1340 (C=S), 3309 (N-H), 1257 (C-O), 1018 (N-N), 418 (Zn-O) and 594 (Zn-N); ^{1}H NMR (DMSO-d$_6$, δ ppm): 11.35 (s, 1H, NH), 8.06 (s, 1H, NH$_2$), 8.20 (s, 1H, NH$_2$), 8.37 (s, 1H, HC=N), 8.92 (s, br, 2H, OH), 7.83 (s, 1H), Aromatic: 7.83 (s, 1H), 7.34 (d, 1H, J = 8.0 Hz.) , 6.80 (d, 1H, J = 8.5 Hz.), 6.62 (1H), 6.32 (t, 1H), 6.23 (s, 1H).

Conclusions

Synthesis and characterization of a terdentate ONS-donor pincer ligand and its coordination compounds with four divalent metal ions, viz., Fe(II), Co(II), Cu(II) and Zn(II), have been carried in non-aqueous medium. The reaction of metal ions with ligand in 1:2 stoichiometry resulted in three types of complexes: one, a hexacordinated octahedral pincer type complex with iron and cobalt, in which the planarity in both the ligands are retained; second, a pentacoordinate trigonal bi-pyramidal compound with zinc in which one ligand coordinates as bidentate and other as tridentate fashion; and the third one is a square planar copper complex, in which both the ligands behave as bidentate one. An *in-silico* study at DFT level in conjugation with physicochemical data affirm that, in the two octahedral complexes, the two ligands extend a right angle with each other through the central metal atom. The formation of hydrogen bonds (O-H) was also detected in the complexes. The copper complex may be regarded as 'molecular hammock', in which both the opposing C=S bonds in the vicinity of the NOCuON square plane were distorted from the planar geometry. The theoretical NMR, infrared and electronic spectra for the ligand and the complexes showed resemblance with the experimental ones, with high values of correlation coefficients. The calculated stability order obtained from HOMO-LUMO gap of the complexes is $Fe(cattsc)_2 < Co(cattsc)_2 < Cu(cattsc)_2 > Zn(cattsc)_2$ that confirms the William–Irving trend. The global reactivity parameters viz., chemical potential (μ), global hardness (η), global softness (S), electrophilicity (ω), and the ionization potential (I), electron affinity (A) and electronegativity (χ) were evaluated and presented in this study. With the help of the results of TDDFT, FMO and fragmentation approaches, all the observed electronic spectra and electronic transitions were assigned. All the complexes displayed intra–ligand ($\pi \rightarrow \pi^*$) transitions. The ligand–metal charge transfer transition was observed for the copper complex. The percent of contribution for the formation of molecular orbitals and involved transitions also detailed in the study. Interestingly, from the selectivity study of the cattsc with several biometal ions, the cobalt recognition could be evolved. An *in-vitro* antibacterial study revealed Cu(cattsc)$_2$ as an effective resistance against *Staphylococcus aureus* and *Escherichia coli* whereas, the cobalt complex is more active against *Bacillus subtilis.* Results of the MIC values for the ligand and its copper complex were found promising, however, their suitability for application on humans need to be validated. Further, an in-depth investigation can explore the biological mechanism with which these molecules act.

Acknowledgment

The authors are thankful to the Department of Chemistry, NIT Kurukshetra for providing the facilities to carry out the research work and are grateful to TEQIP-III for financial support.

Disclosure statement

No potential conflict of interest was reported by the author(s).

References

[1] Kumar, S. M.; Dhahagani, K.; Rajesh, J.; Nehru, K.; Annaraj, J.; Chakkaravarthi, G.; Rajagopal, G. Synthesis, Characterization, Structural Analysis and DNA Binding Studies of Nickel(II)-Triphenylphosphine Complex of ONS Donor ligand - Multisubstituted Thiosemicarbazone as Highly Selective Sensor for Fluoride Ion. *Polyhedron* **2013**, *59*, 58–68. DOI: 10.1016/j.poly.2013.04.048.

[2] Bal-Demirci, T.; Şahin, M.; Kondakçı, E.; Özyürek, M.; Ülküseven, B.; Apak, R. Synthesis and Antioxidant Activities of Transition Metal Complexes Based 3-hydroxysalicylaldehyde-S-Methylthiosemicarbazone. *Spectrochim. Acta A Mol Biomol. Spectrosc.* **2015**, *138*, 866–872. DOI: 10.1016/j.saa.2014.10.088.

[3] Dilović, I.; Rubcić, M.; Vrdoljak, V.; Kraljević Pavelić, S.; Kralj, M.; Piantanida, I.; Cindrić, M. Novel Thiosemicarbazone Derivatives as Potential Antitumor Agents: Synthesis, Physicochemical and Structural Properties, DNA Interactions and Antiproliferative Activity. *Bioorg. Med. Chem.* **2008**, *16*, 5189–5198. DOI: 10.1016/j.bmc.2008.03.006.

[4] Knox, J. J.; Hotte, S. J.; Kollmannsberger, C.; Winquist, E.; Fisher, B.; Eisenhauer, E. A. Phase II Study of Triapine in patients with metastatic renal cell carcinoma: a trial of the National Cancer Institute of Canada Clinical Trials Group (NCIC IND.161)). *Invest. New Drugs* **2007**, *25*, 471–477. DOI: 10.1007/s10637-007-9044-9.

[5] Degola, F.; Morcia, C.; Bisceglie, F.; Mussi, F.; Tumino, G.; Ghizzoni, R.; Pelosi, G.; Terzi, V.; Buschini, A.; Restivo, F. M.; Lodi, T. *In Vitro* Evaluation of the Activity of Thiosemicarbazone Derivatives against Mycotoxigenic Fungi Affecting Cereals. *Int. J. Food Microbiol.* **2015**, *200*, 104–111. DOI: 10.1016/j.ijfoodmicro.2015.02.009.

[6] Kang, I.-J.; Wang, L.-W.; Hsu, T.-A.; Yueh, A.; Lee, C.-C.; Lee, Y.-C.; Lee, C.-Y.; Chao, Y.-S.; Shih, S.-R.; Chern, J.-H. Isatin-*β*-Thiosemicarbazones as Potent Herpes Simplex Virus Inhibitors. *Bioorg. Med. Chem. Lett.* **2011**, *21*, 1948–1952. DOI: 10.1016/j.bmcl.2011.02.037.

[7] Quenelle, D. C.; Keith, K. A.; Kern, E. R. In Vitro and in Vivo Evaluation of Isatin-*β*- Thiosemicarbazone and Marboran against Vaccinia and Cowpox Virus Infections. *Antiviral Res.* **2006**, *71*, 24–30. DOI: 10.1016/j.antiviral.2006.02.010.

[8] Debebe, Z.; Ammosova, T.; Breuer, D.; Lovejoy, D. B.; Kalinowski, D. S.; Kumar, K.; Jerebtsova, M.; Ray, P.; Kashanchi, F.; Gordeuk, V. R.; et al. Iron Chelators of the Di-2-Pyridylketone Thiosemicarbazone and 2-Benzoylpyridine Thiosemicarbazone Series Inhibit HIV-1 Transcription: Identification of Novel Cellular Targets-Iron, Cyclin-Dependent Kinase (CDK) 2, and CDK9. *Mol. Pharmacol.* **2011**, *79*, 185–196. DOI: 10.1124/mol.110.069062.

[9] Pelosi, G.; Bisceglie, F.; Bignami, F.; Ronzi, P.; Schiavone, P.; Re, M. C.; Casoli, C.; Pilotti, E. Antiretroviral Activity of Thiosemicarbazone Metal Complexes. *J. Med. Chem.* **2010**, *53*, 8765–8769. DOI: 10.1021/jm1007616.

[10] Torti, S. V.; Torti, F. M. Iron and Cancer: more Ore to Be Mined. *Nat. Rev. Cancer* **2013**, *13*, 342–355. DOI: 10.1038/nrc3495.

[11] Nehar, O. K.; Mahboub, R.; Louhibi, S.; Roisnel, T.; Aissaoui, M. New Thiosemicarbazone Schiff Base Ligands: Synthesis, Characterization, Catecholase Study and Haemolytic Activity. *J. Mol. Struct.* **2020**, *1204*, 127566. DOI: 10.1016/j.molstruc.2019.127566.

[12] Mauro, C.; Matteo, T.; Jennifer, B.; Giorgio, P.; Cristina, M.; Marika, S.; Dominga, R.; Valentina, G. In Vitro and in Vivo Anticancer Activity of Tridentate Thiosemicarbazone Copper Complexes: Unravelling an Unexplored Pharmacological Target. *Eur. J. Med. Chem.* **2020**, *194*, 112266. DOI: 10.1016/j.ejmech.2020.112266.

[13] Liu, Q.; Xie, B.; Lin, S.; Liao, Q.; Deng, R.; Zhaohua, Y. Silicon-Containing Diorganotin Complexes with Salicylaldehyde Thiosemicarbazone and Their Anticancer Activity. *J. Chem. Sci.* **2019**, *131*, 73. DOI: 10.1007/s12039-019-1650-5.

[14] Sankaraperumal, A.; Karthikeyan, J.; Shetty, A. N.; Lakshmisundaram, R. Nickel(II) Complex of p-[N,N-Bis(2-Chloroethyl)Amino]Benzaldehyde-4-Methyl Thiosemicarbazone: Synthesis, Structural Characterization and Biological Application. *Polyhedron* **2013**, *50*, 264–269. DOI: 10.1016/j.poly.2012.11.006.

[15] Ahmadi, R. A.; Amani, S. Synthesis, Spectroscopy, Thermal Analysis, Magnetic Properties and Biological Activity Studies of Cu(II) and Co(II) Complexes with Schiff Base Dye Ligands. *Molecules* **2012**, *17*, 6434–6448. DOI: 10.3390/molecules17066434.

[16] Jain, P.; Chaturvedi, K. K. Complexes of Cu(II), Ni(II) and Co(II) with Sulphamerazine Salicylaldimine. *J. Inorg. Nucl. Chem.* **1977**, *39*, 901–903. DOI: 10.1016/0022-1902(77)80182-6.

[17] Archer, R. D.; Wang, B. Synthesis and Characterization of the Thermally Stable Copolymer of Tetrakis(salicylaldehydato-O,O')Zirconium(IV) and 3,3'-Diaminobenzidine. *Inorg. Chem.* **1990**, *29*, 39–43. DOI: 10.1021/ic00326a009.

[18] Xiong, R.-G.; Song, B.-L.; Zuo, J.-L.; You, X.-Z.; Huang, X.-Y. Syntheses and Properties of Complexes of Cu^{II}, Ni^{II} and Zn^{II} with N,N'-Trimethylene Bis(Salicylaldehyde Imine). Crystal Structure of of Cu(Sal$_2$tn). *Polyhedron* **1996**, *15*, 903–907. DOI: 10.1016/0277-5387(95)00319-6.

[19] Lemire, J. A.; Harrison, J. J.; Turner, R. J. Antimicrobial Activity of Metals: mechanisms, Molecular Targets and Applications. *Nat. Rev. Microbiol.* **2013**, *11*, 371–384. DOI: 10.1038/nrmicro3028.

[20] Farrugia, K. N.; Makuc, D.; Podborska, A.; Szaciłowski, K.; Plavec, J.; Magri, D. C. UV-visible and (1)H-(15)N NMR spectroscopic studies of colorimetric thiosemicarbazide anion sensors . *Org. Biomol. Chem.* **2015**, *13*, 1662–1672. DOI: 10.1039/c4ob02091j.

[21] Sharma, D.; Moirangthem, A.; Roy, S. M.; Kumar, A. S. K.; Nandre, J. P.; Patil, U. D.; Basu, A.; Sahoo, S. K. Bioimaging

Application of a Novel Anion Selective Chemosensor Derived from Vitamin B6 Cofactor. *J. Photochem. Photobiol. B, Biol.* **2015**, *148*, 37–42. DOI: 10.1016/j.jphotobiol.2015.03.021.

[22] Cametti, M.; Rissanen, K. Highlights on Contemporary Recognition and Sensing of Fluoride Anion in Solution and in the Solid State. Chem. Soc. Rev. **2013**, *42*, 2016–2038. DOI: 10.1039/c2cs35439j.

[23] Suksai, C.; Tuntulani, T. Chromogenic Anion Sensors. Chem. Soc. Rev. **2003**, *32*, 192–202. DOI: 10.1039/b209598j.

[24] Van Koten, G.; Timmer, K.; Noltes, J. G.; Spek, A. L. A Novel Type of Pt-C Interaction and a Model for the Final Stage Stage in Reductive Elimination Processes Involving C-C Coupling at Pt; Synthesis and Molecular Geometry of [l,N,N'-η-2,6-Bis((Dimethylamino)Methyl}- Toluene]Iodoplatinum(II) Tetrafluoroborate. *J. Chem. Soc., Chem. Commun.* **1978**, 250–252. DOI: 10.1039/C39780000250.

[25] Moulton, C. J.; Shaw, B. L. Transition Metal–Carbon Bonds. Part XLII. Complexes of Nickel, Palladium, Platinum, Rhodium and Iridium with the Tridentate Ligand 2,6-Bis[(di-t-Butylphosphino)Methyl]Phenyl. *J. Chem. Soc. Dalton Trans.* **1976**, 1020–1024. DOI: 10.1039/DT9760001020.

[26] Peris, E.; Crabtree, R. H. Key Factors in Pincer Ligand Design. Chem. Soc. Rev. **2018**, *47*, 1959–1968. DOI: 10.1039/c7cs00693d.

[27] Swesi, A. T.; Farina, Y.; Baba, I. Synthesis and Characterization of Some Diorganotin(IV) Complexes of 2,3-Dihydroxybenzaldehyde N(4)- Substituted Thiosemicarbazone. *Sains Malaysiana* **2007**, *36*, 21–26.

[28] Geary, W. J. The Use of Conductivity Measurements in Organic Solvents for the Characterisation of Coordination Compounds. *Coord. Chem. Rev.* **1971**, *7*, 81–122. DOI: 10.1016/S0010-8545(00)80009-0.

[29] Mittapally, S.; Taranum, R.; Parveen, S. Metal Ions as Antibacterial Agents. *J. Drug Deliv. Ther.* **2018**, *8*, 411–419. DOI: 10.22270/jddt.v8i6-s.2063.

[30] Afrasiabi, Z.; Sinn, E.; Chen, J.; Ma, Y.; Rheingold, A. L.; Zakharov, L. N.; Rath, N.; Padhye, S. Appended 1,2-Naphthoquinones as Anticancer Agents 1: synthesis, Structural, Spectral and Antitumor Activities of *Ortho*-Naphthaquinone Thiosemicarbazone and Its Transition Metal Complexes. *Inorg. Chim. Acta* **2004**, *357*, 271–278. DOI: 10.1016/S0020-1693(03)00484-5.

[31] Bindu, P.; Kurup, M. R. P.; Satyakeerty, T. R. EPR, Cyclic Voltammetric and Biological Activities of Copper(II) Complexes of Salicylaldehyde N(4)-Substituted Thiosemicarbazone and Heterocyclic Bases. *Polyhedron* **1998**, *18*, 321–331. DOI: 10.1016/S0277-5387(98)00166-1.

[32] Abd-Elzaher, M. M. Synthesis, Characterization, and Antimicrobial Activity of Cobalt(II), Nickel(II), Copper(II) and Zinc(II) Complexes with Ferrocenyl Schiff Bases Containing a Phenol Moiety. *Appl. Organometal. Chem.* **2004**, *18*, 149–155. DOI: 10.1002/aoc.608.

[33] Tan, K. W.; Seng, H.; Lim, F. S.; Cheah, S. C.; Ng, C. H.; Koo, K. S.; Mustafa, M. R.; Ng, S. W.; Maah, M. J. Towards a Selective Cytotoxic Agent for Prostate Cancer: Interaction of Zinc Complexes of Polyhydroxybenzaldehyde Thiosemicarbazones with Topoisomerase I. *Polyhedron* **2012**, *38*, 275–284. DOI: 10.1016/j.poly.2012.03.014.

[34] Barber, D. E.; Lu, Z.; Richardson, T.; Crabtree, R. H. Silane Alcoholysis by a Nickel(II) Complex in a N, O, S Ligand Environment. *Inorg. Chem.* **1992**, *31*, 4709–4711. DOI: 10.1021/ic00048a049.

[35] Becke, A. D. Density Functional Thermochemistry. III. The Role of Exact Exchange. *J. Chem. Phys* **1993**, *98*, 5648–5652. DOI: 10.1063/1.464913.

[36] Frisch, M. J.; Trucks, G. W.; Schlegel, H. B.; Scuseria, G. E.; Robb, M. A.; Cheeseman, J. R.; Scalmani, G.; Barone, V.; Petersson, G. A.; Nakatsuji, H. Gaussian 09, Revision E.01, Gaussian, Inc., Wallingford CT, **2016**.

[37] Rogolino, D.; Bacchi, A.; Luca, L. D.; Rispoli, G.; Sechi, M.; Stevaert, A.; Naesens, L.; Carcelli, M. Investigation of the Salicylaldehyde Thiosemicarbazone Scaffold for Inhibition of Influenza Virus PA Endonuclease. *J. Biol. Inorg. Chem.* **2015**, *20*, 1109–1121. DOI: 10.1007/s00775-015-1292-0.

[38] Shawish, H. B.; Paydar, M.; Looi, C. Y.; Wong, Y. L.; Movahed, E.; Halim, S. N. A.; Wong, W. F.; Mustafa, M.-R.; Maah, M. J. Nickel(II) Complexes of Polyhydroxybenzaldehyde N4-Thiosemicarbazones: synthesis, Structural Characterization and Antimicrobial Activities. *Trans. Met. Chem.* **2014**, *36*, 81–94. DOI: 10.1007/s11243-013-9777-6.

[39] Data (CCDC 941774) obtained from Cambridge crystallographic data centre, 12 Union Road, Cambridge CB21E2, UK via htt:www.ccdc.cam.ac.uk/conts/retrievinghtml.

[40] Dennington, T. K. R.; Milliam, J. Gaussview, Version 5, Semichem Inc., Shawnee Mission, KS, **2009**, 5.

[41] Zhou, Z.; Parr, R. J. Activation Hardness: New Index for Describing the Orientation of Electrophilic Aromatic Substitution. *J. Am. Chem. Soc.* **1990**, *112*, 5720–5724. DOI: 10.1021/ja00171a007.

[42] Parr, R. G.; Pearson, R. G. Absolute Hardness: Companion Parameter to Absolute Electronegativity. *J. Am. Chem. Soc.* **1983**, *105*, 7512–7516. [Database] DOI: 10.1021/ja00364a005.

[43] Pearson, R. G. Absolute Electronegativity and Hardness Correlated with Molecular Orbital Theory. *Proc. Natl. Acad. Sci. USA.* **1986**, *83*, 8440–8441. DOI: 10.1073/pnas.83.22.8440.

[44] Pearson, R. G. Recent Advances in the Concept of Hard and Soft Acids and Bases. *J. Chem. Educ.* **1987**, *64*, 561–567. DOI: 10.1021/ed064p561.

[45] Parr, R. G.; Chattaraj, P. K. Principle of Maximum Hardness. *J. Am. Chem. Soc.* **1991**, *113*, 1854–1855. DOI: 10.1021/ja00005a072.

[46] Datta, D. Hardness Profile" of a Reaction Path. *J. Phys. Chem.* **1992**, *96*, 2409–2410. DOI: 10.1021/j100185a005.

[47] Pearson, R. G. The Principle of Maximum Hardness. *Acc. Chem. Res.* **1993**, *26*, 250–255. DOI: 10.1021/ar00029a004.

[48] Parr, R. G.; Gazquez, J. L. Hardness Functional. *J. Phys. Chem.* **1993**, *97*, 3740–3939. DOI: 10.1021/j100118a003.

[49] Gázquez, J. L.; Martĭnez, A.; Méndez, A. Relationship between Energy and Hardness Differences. *J. Phys. Chem.* **1993**, *97*, 4059–4063. DOI: 10.1021/j100118a021.

[50] Kar, T.; Scheiner, S.; Sannigrahi, A. B. Hardness and Chemical Potential Profiles for Some Open-Shell HAB → HBA Type Reactions. Ab Initio and Density Functional Study. *J. Phys. Chem. A.* **1998**, *102*, 5967–5973. DOI: 10.1021/jp9809888.

[51] Koopmans, T. A. Ordering of Wave Functions and Eigenenergies to the Individual Electrons of an Atom. *Physica* **1934**, *1*, 104–113. DOI: 10.1016/S0031-8914(34)90011-2.

[52] (a) Weigend, F.; Ahlrichs, R. Balanced basis sets of split valence, triple zeta valence and quadruple zeta valence quality for H to Rn: Design and assessment of accuracy. *Phys. Chem. Chem. Phys.* **2005**, *7*, 3297–3305. DOI: 10.1039/b508541a. (b) Weigend, F. Accurate Coulomb-fitting basis sets for H to Rn. *Phys. Chem. Chem. Phys.* **2006**, *8*, 1057–1065. DOI: 10.1039/b515623h.

[53] Cotton, F. A.; Wilkinson, Geoffrey, Murillo, Carlos, A.; Bochmann, M. *Advanced Inorganic Chemistry*; Wiley-Interscience: New York, **1999**; Vol. 6. ISBN 0-471-19957-5.

[54] Chremos, A.; Douglas, J. F. Communication: When Does a Branched Polymer Become a Particle? J. Chem. Phys. **2015**, *143*, 111104–111104-5. DOI: 10.1063/1.4931483.

[55] Agyare, C.; Antwi Apen, J.; Adu, F.; Kesseih, E.; Duah Boaky, Y. Antibiotic Resistance Modulation and Cytotoxicity Studies of Different Extracts of *Pupalia Lappacea*. *Pharmacologia* **2015**, *6*, 244–257. DOI: 10.5567/pharmacologia.2015.244.257.

[56] Traub, W. H.; Leonhard, B. Detection of Antimicrobial Drugs with *Bacillus subtilis* Strain ATCC 6633: An Update. *Chemotherapy* **1992**, *38*, 155–158. DOI: 10.1159/000238956.

[57] Jeffery, G. H.; Basset, J.; Mendham, J.; Denney, R. C. *Vogel's Textbook of Quantitative Chemical Analysis*, 5th ed.; Longman Scientific & Technical: New York, **1989**; pp 454–490.